QUARTERLY JOURNAL OF THE ROYAL METEOROLOGICAL SOCIETY
Q. J. R. Meteorol. Soc. **133**: 1755–1770 (2007)
Published online 4 October 2007 in Wiley InterScience
(www.interscience.wiley.com) DOI: 10.1002/qj.139

RMetS
ROYAL METEOROLOGICAL SOCIETY

Application of a potential vorticity modification method to a case of rapid cyclogenesis over the Atlantic Ocean

A. M. M. Manders, W. T. M. Verkley,* J. J. Diepeveen and A. R. Moene
Royal Netherlands Meteorological Institute, The Netherlands

ABSTRACT: A method to modify the potential vorticity of a numerical weather analysis is applied to a case of rapid cyclogenesis over the Atlantic Ocean. The development of the cyclone's intensity in terms of mean sea level pressure is underestimated by the Dutch version of the limited-area weather prediction model HIRLAM. The analysis shows a rather clear mismatch between the potential vorticity of the analysis and the corresponding water vapour satellite image. A barotropic displacement of potential vorticity, based on a subjective comparison with the water vapour satellite image, improves the forecast in terms of the cyclone's mean sea level pressure eighteen hours after the analysis. Similar but different modifications are investigated to assess the sensitivity of the development to the modification applied.

The numerical analysis of the global ECMWF model displays a similar mismatch between potential vorticity and water vapour image, although the mismatch is somewhat less dramatic than for the HIRLAM model. Notwithstanding, the ECMWF model describes the development of the mean sea level pressure of the cyclone very well. Investigation of targeted singular vectors and a regular ensemble for this case shows, however, that the forecast is sensitive to perturbations of the initial state, in particular in the region of the potential vorticity/water vapour mismatch. The operational forecast lies in the middle of the ECMWF ensemble, the ensemble containing members with both stronger and weaker development of the cyclone.

Our study confirms that a mismatch between an analysed potential vorticity field and a water vapour satellite image might indicate an error in the analysis. However, the error is not necessarily confined to the upper atmosphere and may involve the lower atmosphere as well. Pairs of ECMWF ensemble members, differing according to the sign of the initial perturbation and leading to either shallow or deep cyclones, are studied to shed some light on the effect of different initial conditions. The modification that improves the HIRLAM forecast resembles one of the more strongly developing ensemble members, indicating that the modification lies within the range of acceptable possibilities.

KEY WORDS numerical weather prediction; HIRLAM

Received 12 July 2006; Revised 25 April 2007; Accepted 11 June 2007

1. Introduction

Although numerical weather prediction models have become increasingly accurate, there are still cases in which extreme weather conditions are predicted at a very late stage, leaving little time to give warnings and take protecting measures. In many cases the quality of the forecast is limited by the accuracy of the initial condition or analysis. The accuracy of the analysis may suffer from a lack of observations or from erroneous rejections of extreme values by the automatic quality control of the data assimilation system. Therefore, numerical weather forecasts need to be monitored by an experienced forecaster who may detect errors in the numerical analysis and forecast system by checking the system against the latest observations. This paper discusses a method that enables a forecaster to modify a numerical weather analysis and rerun the numerical model if such a check gives reason to do so.

The information on which a decision to modify a numerical weather analysis might be based could be provided by radiance measurements in the 6.2 μm water vapour absorption channel, as obtained from satellites like METEOSAT-8. Dark and light patterns on a water vapour image, corresponding to high and low values of the brightness temperature, can be related to structures in the potential vorticity field. Potential vorticity has low values in the troposphere (0–2 PVU; 1 PVU = $10^{-6}\mathrm{m^2 s^{-1} K\ kg^{-1}}$) but rapidly increases with height in the stratosphere. The region in which the potential vorticity increases rapidly from 1 to 3 PVU is generally associated with the tropopause. Due to hydrostatic and geostrophic balance, valid for the synoptic-scale weather phenomena in which we are interested, depressions can be associated with isolated low tropopause areas, whereas jet streams go together with elongated regions in which the tropopause slopes steeply. Now, to a first approximation, the brightness temperature displayed in

* Correspondence to: W. T. M. Verkley, Royal Netherlands Meteorological Institute, PO Box 201, 3730 AE De Bilt, The Netherlands.
E-mail: verkley@knmi.nl

a water vapour satellite image is determined by the temperature of the tropopause and varies roughly between 200 and 250 K. A localized area with high values of the brightness temperature (dark spot in a satellite image) thus corresponds to a low tropopause area. Such an area, in turn, would show up as a localized region of high potential vorticity if the latter is displayed on a quasi-horizontal surface like a surface of constant pressure (isobaric surface) or a surface of constant potential temperature (isentropic surface). Likewise, an elongated region with sharp contrasts in brightness temperature (sharp contrasts in grey shades) would go along with a region in which the tropopause slopes steeply, and in that case the potential vorticity on a quasi-horizontal surface would show large horizontal gradients.

It follows that the location of depressions and the jet stream in a numerical weather analysis can be checked against reality by comparing these with the corresponding structures in the water vapour satellite image. Some care should be taken, however, since the correspondence is not one-to-one. Water vapour satellite images may, for example, show traces of clouds higher in the atmosphere. In that case the observations do not fully represent tropopause conditions. Despite these limitations, comparing water vapour satellite images with potential vorticity fields could lead to the detection of errors in the analysis. Taking for granted that a particular modification of the potential vorticity is then appropriate, the invertibility principle guarantees that pressure, wind and temperature fields are modified accordingly and in a dynamically consistent way. These and further properties of potential vorticity are discussed thoroughly by Hoskins *et al*. (1985). Inversion of potential vorticity is applied by Davis and Emanuel (1991) and Demirtas and Thorpe (1999). An extensive treatment of the interpretation of potential vorticity and water vapour images with many examples can be found in Santurette and Georgiev (2005).

The idea to modify a numerical weather analysis based on comparing potential vorticity with water vapour images was applied successfully by Demirtas and Thorpe (1999) in a few case-studies. But in the follow-up study by Swarbrick (2001), it appeared that it is extremely difficult to find a quantitatively correct potential vorticity modification since every case is different. A way to get a more quantitative hold on the potential vorticity modifications is to use singular vectors. Røsting *et al*. (2003) tested this for the 1997 Christmas storms using the Norwegian version of the High-Resolution Limited-Area Model (HIRLAM). They used singular vectors from the European Centre for Medium-Range Weather Forecasts (ECMWF) model to identify modifications which have significant impact on the forecast. In a later publication, Røsting and Kristjánsson (2006) applied their method to a few winter storms in 1999 and 2000. However, the merits of the method remain a subject of debate and more case-studies are needed to assess its usefulness in practice.

In the present study we use the method developed by Verkley *et al*. (2005) in studying a case in which the operational HIRLAM analysis clearly shows a mismatch with the water vapour satellite image, and in which the subsequent deepening of a cyclone, as simulated by HIRLAM, is too weak when compared with verifying analyses. We will discuss a modification that improves the match with the water vapour satellite image and leads to a better prediction of the developing cyclone. The modified analysis and forecast are compared, variations in the modification parameters are discussed and an ensemble of forecasts by ECMWF is studied to address the question of why the modification has been successful. In section 2 the method of potential vorticity modification is summarized, after which a description of the case is given in section 3. Then the modification is discussed, with attention to the effect on the initial state and subsequent dynamical development. Several alternative modifications are applied to test the sensitivity of the development to the modification parameters. The results will be compared with the ECMWF forecast and targeted singular vectors as well as with an ensemble of 50 alternative forecasts in section 4. Section 5 discusses the merits and problems of our approach and section 6 concludes the paper.

2. The method

In the hydrostatic approximation and for a coordinate system in which potential temperature, θ, is used as a height variable, the expression for potential vorticity, P, reads

$$P = -g(f + \zeta_\theta)\left(\frac{\partial \theta}{\partial p}\right),$$

where g is the acceleration due to gravity, f is the Coriolis parameter, ζ_θ is the relative vorticity in θ coordinates and p is pressure. Using the rules for transformation between different vertical coordinate systems (e.g. Haltiner and Williams, 1980), the corresponding expression in the η-coordinate system of HIRLAM is

$$P = -g\left\{(f+\zeta_\eta)\frac{\partial \theta}{\partial p} - \frac{1}{a\cos\phi}\frac{\partial v}{\partial p}\left[\frac{\partial \theta}{\partial \lambda}\right]_\eta + \frac{1}{a}\frac{\partial u}{\partial p}\left[\frac{\partial \theta}{\partial \phi}\right]_\eta\right\}. \quad (1)$$

The horizontal coordinates are longitude, λ, and latitude, ϕ, and the two components of the horizontal velocity are u and v. The mean radius of the earth is denoted by a. Horizontal and vertical derivatives are approximated by centred finite differences based on the computational grid of HIRLAM.

The modification is based on a comparison of the water vapour image with the potential vorticity on an isentropic surface. Ideally, the isentropic surface should intersect the tropopause where it has the steepest slopes. This leads to 315 K as a reasonable choice for midlatitudes in winter and to 330 K in summer (Hoskins *et al*., 1985). When there is a mismatch, the potential vorticity field can be modified by a graphical interface

DOI: 10.1002/qj

in terms of pre-defined modifications: the addition of a source/sink, the strengthening/weakening of a structure and the displacement of a structure. All modifications are defined on circular regions of variable radius b in the horizontal. The modification is strongest in the centre of the circle and falls off with increasing distance, r, from the centre to guarantee continuity, according to

$$\mathcal{G}(r; b, \alpha) \equiv \exp\left\{(\ln\ \epsilon)\left(\frac{r}{b}\right)^{2\alpha}\right\}, \quad 0 \le r \le b. \quad (2)$$

The steepness parameter α determines how the modification falls off with r. For $\alpha = 1$ the profile is Gaussian; for $\alpha > 1$ the top of the peak is broader and the side-wings are steeper than for a Gaussian profile. The parameter ϵ is set to 5×10^{-5} to make sure that no large discontinuities across the boundary of the modified area will arise. For the displacement, a simple advection scheme is applied in such a way that no disruptions of the surroundings occur.

Modifications are not uniform in the vertical. For the strengthening and addition of a source/sink, the vertical extent of the modification must be limited. Otherwise, modifications would become too strong with respect to the ambient potential vorticity in the high stratosphere (strengthening) or in the low troposphere (source). The same type of structure function $\mathcal{G}$ is used to constrain the modification to a limited set of model levels, centred around the tropopause, with a different set of parameters than for the horizontal. This is different from the vertical structure function as proposed by Verkley *et al.* (2005). The precise structure in the vertical is still a point of discussion and the ideal configuration may change from case to case. The vertical extent of the modifications in the literature is mostly between 300 and 700 hPa to represent the local change in tropopause topography.

We use version 6.3.5 of HIRLAM, operational at the Royal Netherlands Meteorological Institute (KNMI) until autumn 2006. It has a horizontal resolution of 22 km on a rotated coordinate system of which the equator runs through the centre of the computational domain. In the vertical, 40 η-levels are used. Details of the model can be found in Undén *et al.* (2002). To modify a HIRLAM analysis, the modification parameters (coordinates, radius, type, strength, steepness) are read by HIRLAM and the potential vorticity field is modified directly on the HIRLAM grid. Previously, an externally modified potential vorticity field was used as input, but it was realized later that interpolation to the HIRLAM grid generates some noise that reduces the efficiency of the numerical procedure.

Instead of inverting the modified potential vorticity and assimilating the modified fields of pressure, wind and temperature, the modified potential vorticity field is assimilated directly by the variational data assimilation scheme (3D-Var) to generate a new analysis for the full set of dynamical variables. For details on the implementation of 3D-Var in HIRLAM, see Gustafsson *et al.* (2001) and Lindskog *et al.* (2001). In terms of standard terminology, we minimize the cost function $J = J_\mathrm{b} + J_\mathrm{p}$, where the terms J_b (background) and J_p (potential vorticity) are:

$$\left.\begin{aligned} J_\mathrm{b} &= \tfrac{1}{2}[\mathbf{x} - \mathbf{x}_\mathrm{b}]^\mathrm{T}\mathbf{B}^{-1}[\mathbf{x} - \mathbf{x}_\mathrm{b}], \\ J_\mathrm{p} &= \tfrac{1}{2}[\mathcal{F}(\mathbf{x}) - \mathbf{z}]^\mathrm{T}\mathbf{W}^{-1}[\mathcal{F}(\mathbf{x}) - \mathbf{z}]. \end{aligned}\right\} \quad (3)$$

Here $\mathbf{x}$ is the model state, $\mathbf{x}_\mathrm{b}$ the background state, $\mathcal{F}(\mathbf{x})$ the operator that calculates the potential vorticity field from the model state $\mathbf{x}$, and $\mathbf{z}$ is the modified potential vorticity field. For the background covariance matrix $\mathbf{B}$, we use the same matrix as the one used in the assimilation of conventional observations. For the potential vorticity covariance matrix $\mathbf{W}$, we choose a simple diagonal matrix with variances proportional to the squared potential vorticity field of the background. By giving the term J_p a much larger weight than the term J_b in the total cost function, the modified analysis can be made to have a potential vorticity field that is very close to the modified potential vorticity field. Details can be found in Verkley *et al.* (2005).

In our setting, the potential vorticity of the resulting analysis resembles the modified potential vorticity field fairly well. Some small differences are present, depending on the kind of modification. Also some noise is introduced; it seems that the minimization process has some difficulties with strong, localized, isolated perturbations. When a strengthening is applied, convergence is easily reached; for a source or sink the number of iterations needed for convergence is substantially larger. For a displacement, the convergence criterion is hardly ever met. Despite the fact that the convergence criterion on the gradient of the cost function is not always reached within an acceptable number of iterations, the potential vorticity of the resulting analysis does not differ dramatically from the modified potential vorticity field and there are no obvious differences between cases in which the minimum is reached and cases in which it is not.

3. Modifications of HIRLAM analysis and ensuing forecasts

On 7 November 2005, 00 UTC, a wave at upper levels developed in the left exit region of the jet stream over the North Atlantic Ocean, around 46 °N, 30 °W; water vapour images at 00, 06 and 18 UTC are displayed in Figure 1 and show a sequence which is typical for rapid cyclogenesis. The case has been selected on the basis of guidance reports by forecasters at KNMI. It was noticed that, at 00 UTC, the potential vorticity field on the 315 K isentrope shows a clear mismatch with the corresponding water vapour image, as can be seen from Figure 2(a). In the image a cloud head and a dry intrusion are observed without corresponding structures in the potential vorticity field (e.g. Santurette and Georgiev, 2005). The mismatch in the potential vorticity field consists of the following features:

DOI: 10.1002/qj

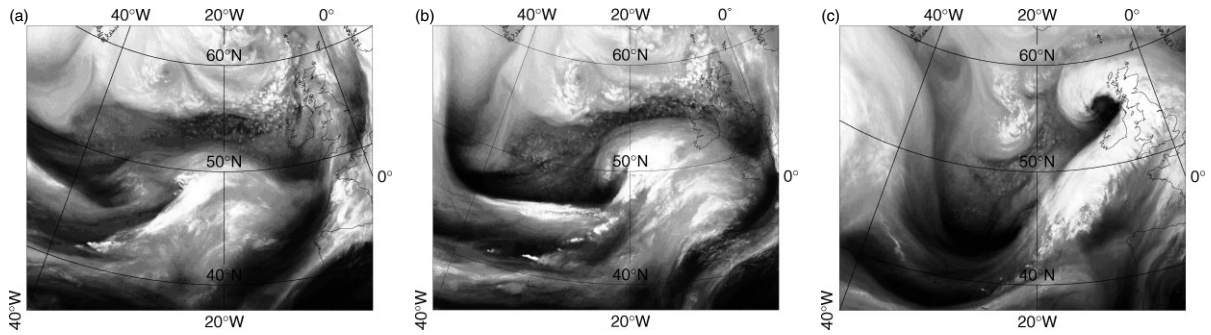

Figure 1. Water vapour satellite images, in the 6.2 μm channel from METEOSAT-8, for 7 November 2005 at (a) 00, (b) 06 and (c) 18 UTC. The grey shades show brightness temperatures in the range from (approximately) 218 K (white) to 240 K (black).

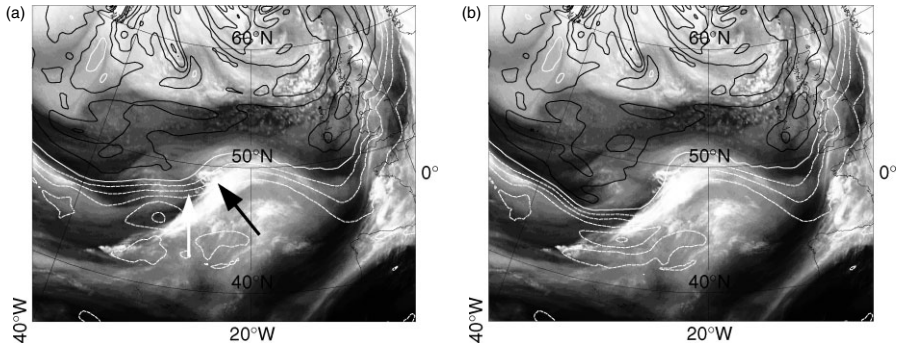

Figure 2. Contours of potential vorticity on the 315 K isentropic surface of the HIRLAM analysis of 7 November 2005, 00 UTC, over the corresponding water vapour image (grey shading). The potential vorticity contour interval is 1 PVU; the white contour denotes 4 PVU, the black contours denote values larger than 4 PVU and the white dashed contours those less than 4 PVU. (a) shows the original HIRLAM analysis, and (b) the analysis resulting from the most successful modification (exp1). In (a), the white arrow indicates the dry intrusion, and the black arrow the cloud head.

1. Enhanced gradients in potential vorticity (jet stream) are too far north.
2. The maximum in potential vorticity in the dry intrusion area is lacking.
3. The minimum in potential vorticity in the cloud-head region is lacking.

HIRLAM analyses at the same times as the water vapour images, i.e. at 00, 06 and 18 UTC, are shown in Figure 3(a–c). At 00 UTC, close to the position of the mismatch, the minimum mean sea level (msl) pressure is, according to the HIRLAM analysis, 1003.8 hPa. The operational run, depicted in Figure 3(d–f), predicts a developing low with a msl pressure of 984.3 hPa after 18 hours (7 November, 18 UTC) to the northwest of Ireland. However, as the analyses show, the actual development is more dramatic, with a msl pressure of 974.9 hPa after 18 hours. At 18 UTC the cyclogenesis is close to its final stage; this time will be used as our verification time.

Using the technique described in the previous section, we applied several modifications to the HIRLAM analysis of 7 November 2005, 00 UTC. The parameters of the modifications and the properties of the analysis and forecasts in terms of location and central pressure of the cyclone can be found in Tables A.I and A.II. The most successful modification in terms of location and msl pressure is denoted by exp1 and consists of a barotropic displacement of potential vorticity in a circular area of radius $b = 8°$, $\alpha = 2$, from 48.8 °N, 32.0 °W to 46.0 °N, 30.3 °W. The analysis that results from the 3D-Var is shown in Figure 2(b). The modification has moved the jet stream locally to the south, resulting in a trough that matches better with the corresponding feature in the water vapour image. Essentially, point 1 of the mismatch is repaired, with a slight additional reduction of the potential vorticity in the cloud-head region (point 3) and somewhat higher potential vorticity values in the dry intrusion (point 2).

The resulting pressure development is shown in Figure 3(g–i). The initial msl pressure in the area of the mismatch is lower by several hPa than the HIRLAM analysis. Checking against a few pressure measurements from ships at 00 UTC (to be discussed later) shows that this brings the analysis closer to the observations at the sea surface. During the development, the msl pressure at 06 UTC is much lower than the HIRLAM analysis but it is close to the analysis value at 18 UTC. The deepening of the depression in the forecast resulting from the modified analysis levels off after 24 h. The path of the cyclone has not changed significantly. The new forecast is a substantial improvement over the original forecast in terms of msl pressure. Pressures at the centre of the developing cyclone are shown in Figure 4(a). In the next subsection we will study the difference between the modified and unmodified runs in more detail.

DOI: 10.1002/qj

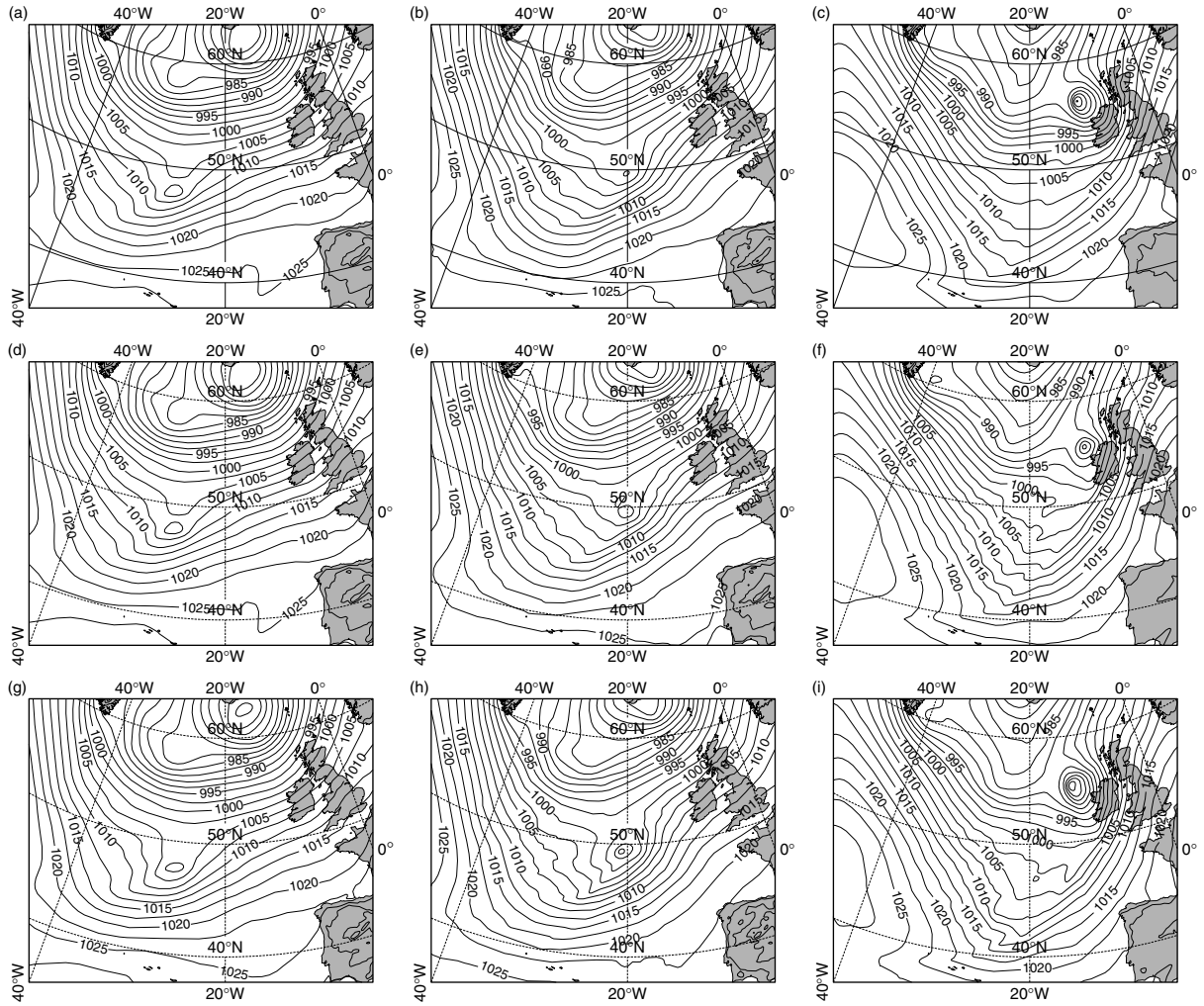

Figure 3. HIRLAM analyses of msl pressure (hPa) for 7 November 2005 at (a) 00 UTC, (b) 06 UTC and (c) 18 UTC; (d–f) show HIRLAM analysis and ensuing forecasts at the same times; (g–i) show modified HIRLAM analysis and ensuing forecasts.

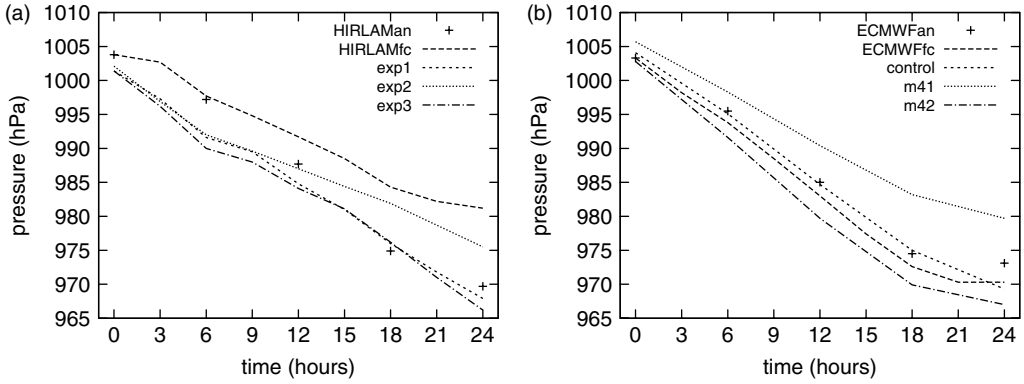

Figure 4. Mean sea level pressure at the cyclone's centre. (a): HIRLAM analyses and forecast and the modified runs exp1, exp2 and exp3, from 3-hourly values. (b): ECMWF analyses and forecast and the control forecast and members 41 and 42 of the ECMWF ensemble, from 6-hourly values.

3.1. Dynamical analysis

The barotropic shift of the potential vorticity field in exp1 has resulted in a local increase of potential vorticity at the 315 K isentropic surface and a local decrease of potential vorticity at model level 34 (around 925 hPa). This can be seen in Figures 5(a) and (d), respectively. The change expresses itself in an increase of cyclonality of the flow. This is demonstrated by the difference fields for the wind in Figures 5(b) and (e) and is consistent with

DOI: 10.1002/qj

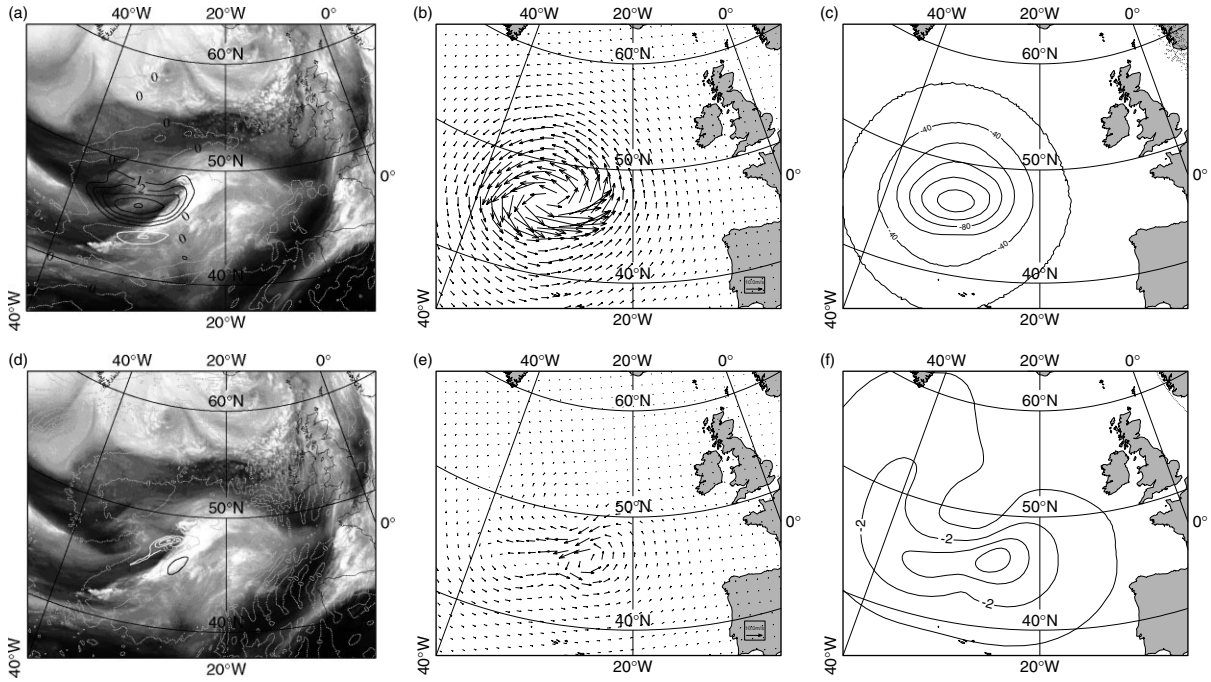

Figure 5. Difference fields at analysis time between modified and unmodified analysis: (a) potential vorticity on 315 K surface, (b) wind at model level 13 (about 300 hPa), (c) geopotential height at 300 hPa, (d) potential vorticity at model level 34 (about 925 hPa), (e) wind at model level 34 (about 925 hPa) and (f) msl pressure. Units are PVU (potential vorticity), metres (geopotential height) and hPa (msl pressure). The unit vector (shown over Iberia) in the wind plots denotes 10 m s^{-1}.

the difference fields of geopotential height at 300 hPa and msl pressure in Figures 5(c) and (f). The modification has also induced a local dipolar change of temperature at model level 13 (around 300 hPa) due to the shift of cold air to the south. At sea level the modification has induced a small decrease in temperature over a large area. These changes are of the order of 1 K and are not shown.

Figure 6 shows the horizontal structure of the potential vorticity field of the analysis and of the +6 h and +18 h forecasts on the 315 K isentropic level. Figure 7 shows the same fields on model level 34 (around 925 hPa). In both the original and modified runs, a strong ridge develops over the British Isles with isolated potential vorticity structures at 315 K equatorward of the jet stream. At analysis time, a small-scale but rather strong low-level potential vorticity structure is present in the original analysis. This structure is very weak in the modified run at analysis time – also evident from the difference field shown in Figure 5(d) – but at +6 h it is already stronger than in the original HIRLAM run. The position of the low-level potential vorticity structure is marked by the crosses in Figures 6 and 7. Vertical cross-sections along latitude circles through these points are shown in Figure 8. Taken together, these figures give a near-complete view of the three-dimensional potential vorticity structure of the modified and unmodified runs. The basic difference between the runs is that the potential vorticity at lower levels, despite the smaller values initially, have become larger in the modified run. At upper levels, the potential vorticity is characterized by the development of a somewhat more pronounced ridge over the British Isles.

Apparently, the modification that we applied has changed the analysis in such a way that both upper and (predominantly) lower structures in the potential vorticity field were able to acquire larger amplitudes. The larger growth of the low-level potential vorticity in the modified run goes together with a larger release of latent heat. To illustrate this, the cumulative precipitation in intervals of three hours is plotted in Figure 9. The position of the low-level structure at 00 UTC, +6 h and +18 h is here also denoted by a cross. Since the precipitation is a time-integrated quantity, one cannot expect an exact match. Still, apart from the first time interval, the position of maximum rainfall and position of the low-level potential vorticity structure correspond very well. For the original HIRLAM analysis and forecast, the maximum precipitation in the cyclogenesis area is 12 mm (0–3 h), 10 mm (3–6 h) and 12 mm (15–18 h), and for the modified run the corresponding values are 20 mm, 14 mm and 12 mm. The much larger rainfall for the modified analysis and forecast in the first few hours, with the corresponding release of latent heat, is consistent with the rapid growth of the low-level anomaly in the first 6 hours. Our case is possibly a moderate version of the 1999 Christmas storm 'Lothar', for which release of latent heat was shown by Wernli *et al*. (2002) to have been a crucial ingredient in its strong development.

3.2. Alternative modifications

Two different forecasters, confronted with the same mismatch between potential vorticity field and water vapour

DOI: 10.1002/qj

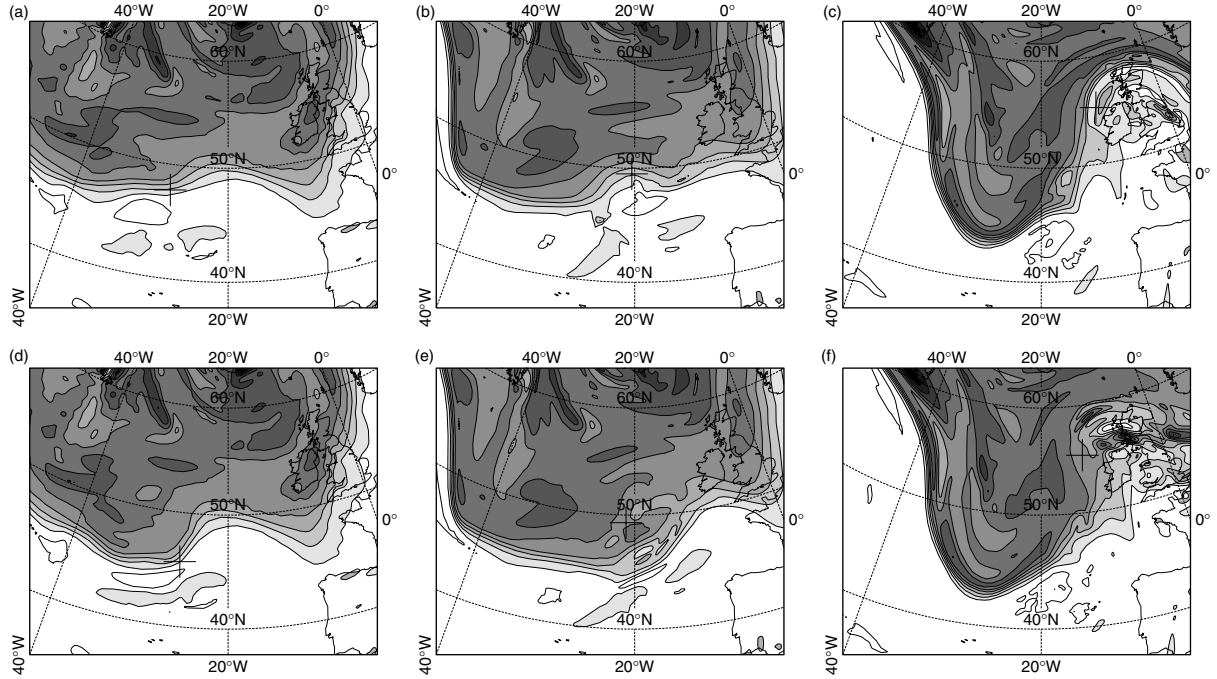

Figure 6. Potential vorticity at the 315 K isentropic level: (a) original analysis and (b) +6 h and (c) +18 h forecasts by HIRLAM, starting from the original analysis; (d) modified analysis and (e) +6 h and (f) +18 h forecasts by HIRLAM, starting from the modified analysis. The contour interval is 1 PVU, with shading above 1 PVU. Crosses indicate the position of the low-level potential vorticity structure, shown in Figure 7.

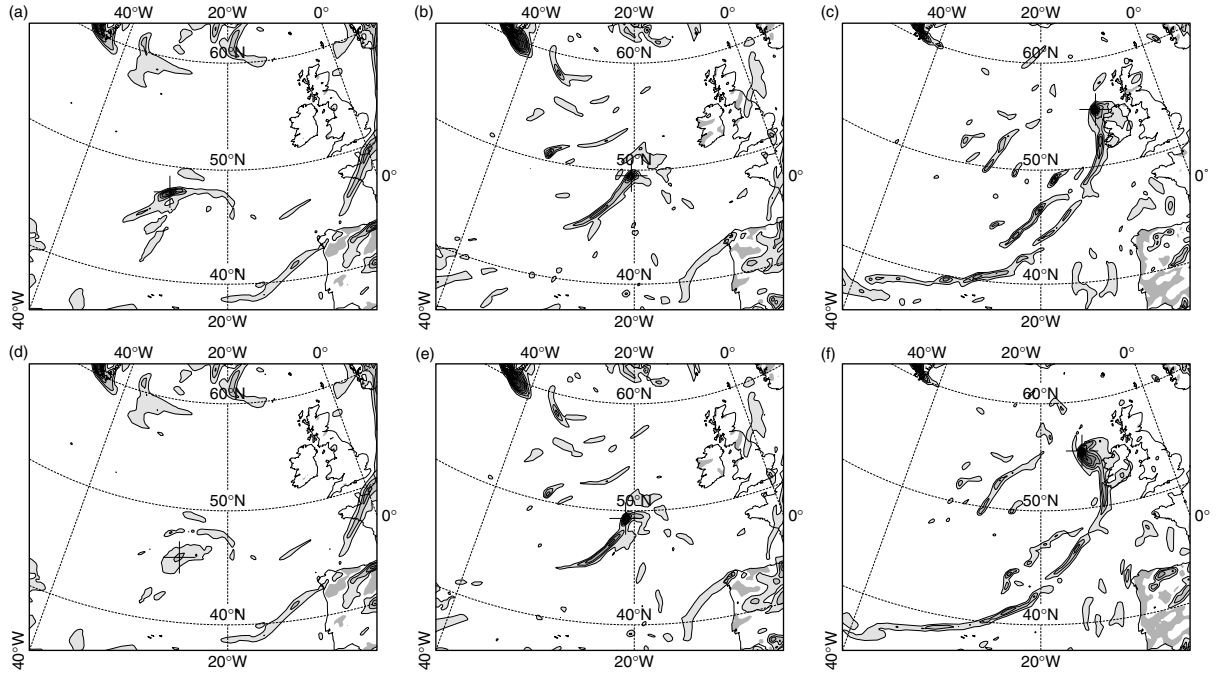

Figure 7. As Figure 6, but showing potential vorticity at model level 34 (around 925 hPa). The contour interval is 0.5 PVU, from 0.5 to 5 PVU, with shading above 0.5 PVU.

image, are not expected to apply the same modification to the analysis. In our case the mismatch is clear enough to result in the same type of modification – a local southward shift of the jet stream – but there will be differences. To test the robustness of the results with respect to the chosen modification, two alternative modifications are applied, denoted by exp2 and exp3. The parameters of these modifications are given in Table A.I. The development of the msl pressure is summarized in Table A.II and displayed graphically in Figure 4(a). Difference fields at analysis time and at +18 h are displayed in Figure 10.

Exp2 is a modification similar to the original modification (exp1) but with a somewhat larger radius and located

DOI: 10.1002/qj

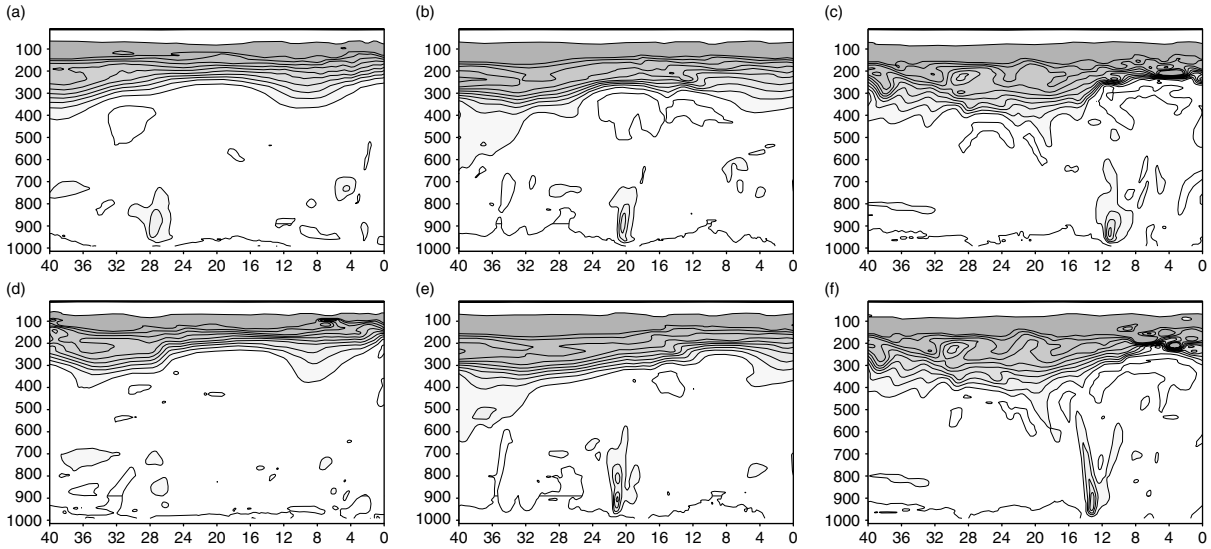

Figure 8. Vertical cross-sections (from 40 °W to 0 °W) of potential vorticity at model levels (translated into approximate pressure levels on the vertical axis) for the original analysis and forecast at (a) analysis time at 47.7 °N, (b) +6 h at 49.5 °N and (c) +18 h at 55.2 °N. (d–f) are as (a–c), but for the modified analysis and forecast at (d) 45.6 °N, (e) 49.3 °N and (f) 55.3 °N. The contour interval (over the range 0–10 PVU) is 1 PVU; an additional contour is shown at 20 PVU.

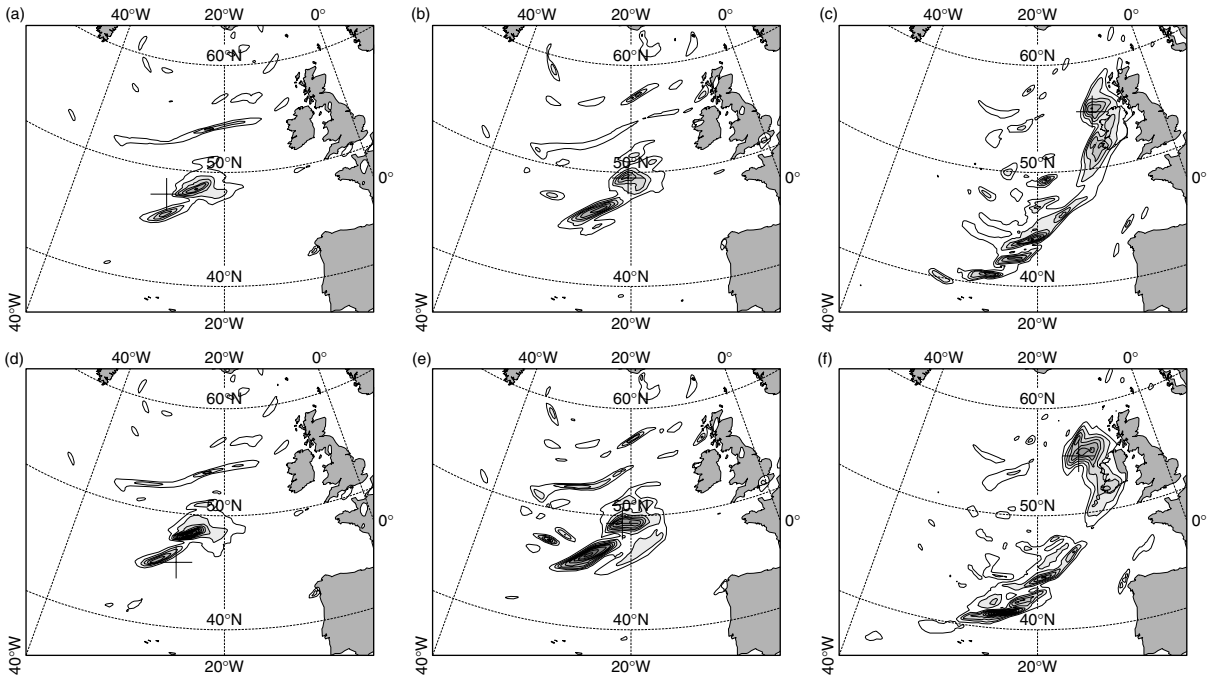

Figure 9. Total precipitation from original analysis and forecast for forecast intervals (a) 0–3 h, (b) 3–6 h and (c) 15–18 h. (d–f) are as (a–c), but for modified analysis and forecast. The contour interval is 2 mm, with the zero contour omitted.

more to the west. The jet stream has been displaced 1° more to the south and the curvature of the jet stream has changed a little. Now, after a similar evolution initially, the development becomes too weak after 12 hours, as can be seen clearly from Figure 4. In addition, the msl pressure pattern of the cyclone becomes elongated instead of circular and it ends up too far to the west. The pressure development is better than in the original forecast in the sense that the value of the msl pressure in the centre is lower, but this goes at the expense of a less correct position of the depression at +18 h. Exp3 is a displacement with the same radius as exp2 but over a slightly smaller distance and starting slightly northward of the original modification. The development of the pressure is now very close to exp1, with slightly lower pressures. The differences in msl pressure with respect to exp1 are not significant.

We also applied a number of modifications that are based on a more systematic variation of the parameters from exp1. Their parameters and msl pressure development are given in Tables A.I and A.II. Four of them (exp1a to exp1d) are shifted versions of exp1, with radius

DOI: 10.1002/qj

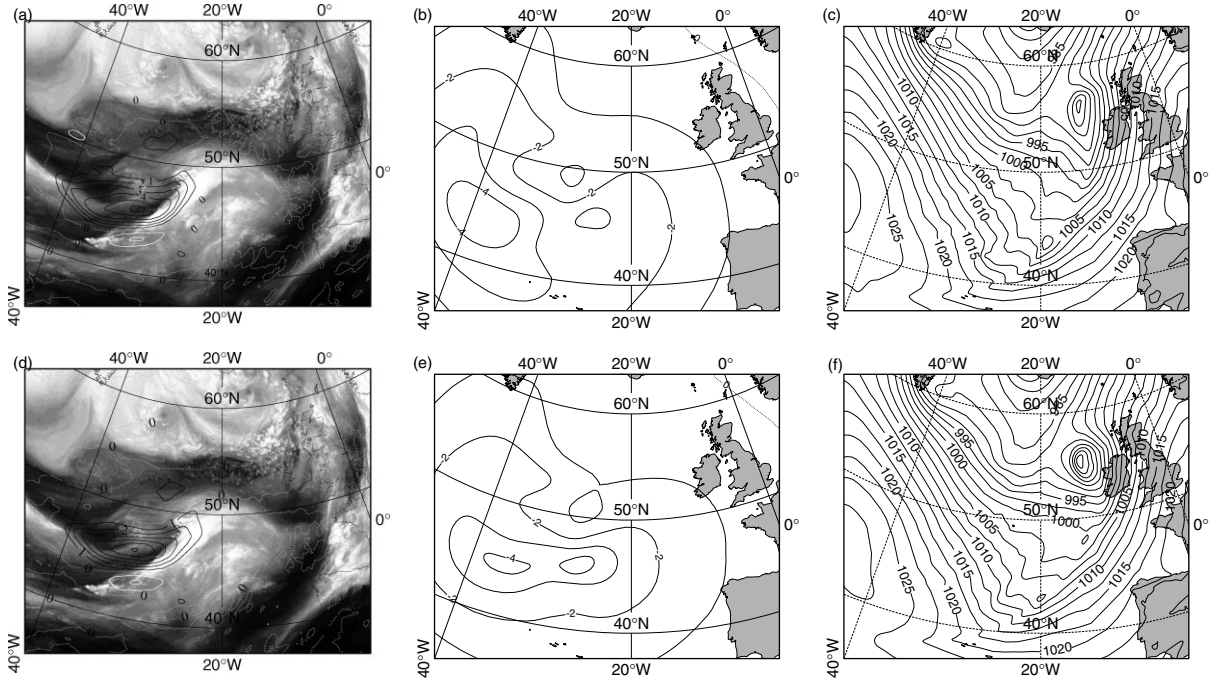

Figure 10. Difference fields for two alternative modifications: (a) potential vorticity at 315 K and (b) msl pressure, both for exp2 at analysis time. (d–e) are as (a–b), but for exp3. (c) and (f) show the +18 h forecast of msl pressure, for exp2 and exp3 respectively; these may be compared with Figures 3(c), (f) and (i). The units are as before.

and displacement equal to exp1 but with different starting points. The other two, trop1 and trop2, are equal to exp1 with the difference that only the upper troposphere and lower stratosphere are displaced. In these cases, for the vertical structure a similar exponential decay function is used as in the horizontal. The small variations in displacement in exp1a to exp1d give small differences in the intensity of the development and in the track of the depression. The decrease in msl pressure with time is not constant and is different for all runs. The pressure development in trop1 and trop2 is not as strong as for the other runs (albeit stronger than for the unmodified run, especially at +24 h).

Due to a different vertical structure function, the potential vorticity at lower levels is not affected in the modifications denoted by trop1 and trop2. This is quite different for exp1a to exp1d, where in some cases the low-level potential vorticity structure nearly disappears. In the original analysis the low-level potential vorticity is about 2.5 PVU. For exp1, exp3 and exp1c it is reduced to about 1 PVU and for exp2, exp1a, exp1b and exp1d it is reduced further to 0.5 PVU, with the smallest values for exp1d. Somewhat unexpectedly, the depression becomes stronger for the cases in which the low-level anomaly is reduced more. The situation appears to be rather complex and suggests that the mutual spatial relationship between the different structures in potential vorticity is as important as their strength. It is noticed, however, that almost all modifications that lead to deeper depressions at +18 h and +24 h are characterized by lower msl pressures in the centre of the incipient cyclone at analysis time. In the next sections we will come back to these issues.

4. Singular vectors and ensemble of ECMWF forecasts

As an alternative way to obtain insight into the role of the potential vorticity structures at analysis time, we consider the case from the perspective of the global ECMWF forecast model. The ECMWF msl pressures at analysis time and at +6 h and +18 h are shown in Figure 11(a–c). Figure 4(b) shows the msl pressures at the cyclone's centre. When assessed in terms of msl pressure, the ECMWF model predicts the evolution of the cyclone better than the HIRLAM model. However, the match between the potential vorticity field and the water vapour image is only slightly better than for the HIRLAM analysis, as can be seen by comparing Figure 12(a) with Figure 2(a). Apparently, the flow at lower levels in the ECMWF analysis is such that, in combination with the flow at upper levels, it produces a realistic development of the msl pressure despite the mismatch at upper levels.

We will see in the next two subsections that the development according to the ECMWF model is rather sensitive to perturbations of the analysis in the region of the mismatch. This will first be explored by studying singular vectors targeted around Great Britain and Ireland, the area where the depression ends up after 24 hours. After that we will study an ECMWF ensemble based on operationally used singular vectors, but without perturbations in the physics parametrizations. Singular vectors and an ensemble are calculated using the PrepIFS system (www.ecmwf.int/services/prepifs) with the ECMWF model at resolution T255 L40. It is implicitly assumed

DOI: 10.1002/qj

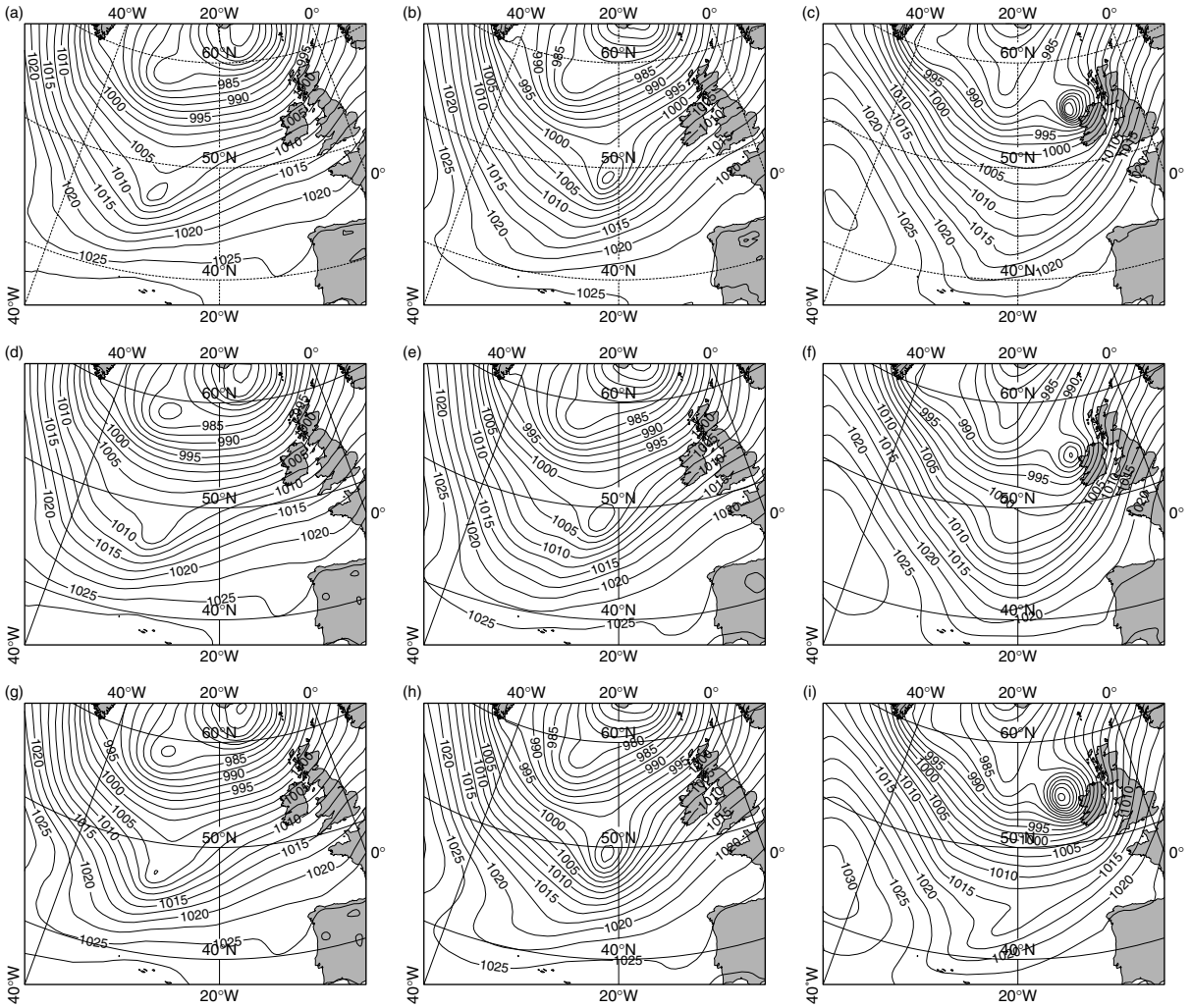

Figure 11. ECMWF global model msl pressure (hPa) analysis at (a) 00 UTC and forecasts at (b) +6 h and (c) +18 h. (d–f) are as (a–c), but for ECMWF ensemble member 41. (g–i) are as (a–c), but for ECMWF ensemble member 42. The ensemble members differ according to the sign of the initial perturbation.

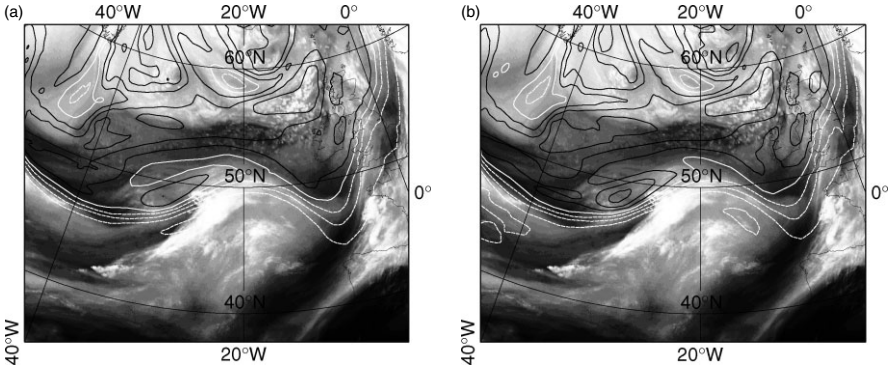

Figure 12. Contours of potential vorticity on the 315 K isentropic surface for the analysis of 7 November 2005, 00 UTC, with the corresponding water vapour image. (a) is from the control run in the ECMWF ensemble, and (b) is for member 42 of the ECMWF ensemble, the second of a pair of ensemble members that give either a weak (41) or strong (42) surface low at +18 h. The contouring convention is as in Figure 2.

that the calculation of singular vectors and the construction of an ensemble are not crucially dependent on the model that is used. Ideally, of course, HIRLAM should be used for this purpose but at the time of writing this was not yet possible.

4.1. Singular vectors

Singular vectors are perturbations of an initial state which give maximum growth over a certain area after a certain amount of time (Buizza and Palmer, 1995). They can be

DOI: 10.1002/qj

related to regions of baroclinic instability (Hoskins *et al*., 2000). The idea of using singular vectors in the context of our work is inspired by the work of Røsting *et al*. (2003) who base their potential vorticity modifications on the structure of the singular vectors on different pressure levels. Apart from modifications in the upper levels of the atmosphere (300–700 hPa), which contribute most to the improvement of the forecast, their singular vectors additionally indicate regions near the surface where the forecast is sensitive. Røsting *et al*. (2003) report that modifications near the ground may indeed lead to a small further improvement of the forecast.

The singular vectors that will be discussed here are calculated for the target area Great Britain and Ireland (20 °W–5 °E, 50 °N–65 °N) and for an optimization time of 24 h. In terms of relative vorticity, the first two singular vectors are shown in Figure 13. Figures 13(a) and (d) show the vertical structure of the singular vectors, Figures 13(b) and (e) the singular vectors at initial time on model level 13 (around 300 hPa), and Figures 13(c) and (f) the singular vectors at the same level at optimization time (24 hours). The growth rates for these vectors is around 100 and indicate that the forecast is quite sensitive to perturbations of the analysis. In addition, the vertical cross-sections of the singular vectors show that the sensitivity has a rather deep vertical structure with a maximum in the neighbourhood of model level 22 (around 600 hPa). The singular vectors, particularly the second one, also show that near the ground the sensitivity can be quite substantial. Both singular vectors indicate that the perturbations with the largest impact on the forecast should have a considerable horizontal scale. This corroborates our findings that modifications of an area of 5° or smaller do not yield significant alterations of the development. The second singular vector has a maximum around 50 °N, 30 °W, which indicates that the area of the potential vorticity/water vapour mismatch is also an area of enhanced sensitivity.

4.2. Ensemble of forecasts

At ECMWF, an ensemble of 50 alternative forecasts is generated to quantify the effect of uncertainties in the analysis (e.g. Molteni *et al*., 1996). The different perturbations of the initial state are based on singular vectors that are designed for optimal growth in a period of 48 hours in the midlatitudes of both the Northern and Southern Hemispheres (Leutbecher and Palmer, 2007). Despite the fact that the singular vectors underlying the standard ECMWF ensemble are not tailored to our small area of interest, the ensemble appears to be relevant for this study. The ensemble members are clearly different in the region of interest at 00 UTC. All members have a local maximum in potential vorticity near 47 °N, 31 °W at the 315 K level, but with differences in strength, size and exact position. Also the position and curvature of the jet stream show some variation. The resulting forecasts show a spread in the position of the depression and the msl pressure at the centre of the depression. At analysis time, the msl pressure is between 1000.6 and 1006.5 hPa, and after 24 hours it is between 959.6 and 982.1 hPa.

The most extreme values in msl pressure at the cyclone centre at +18 h are obtained for ensemble members

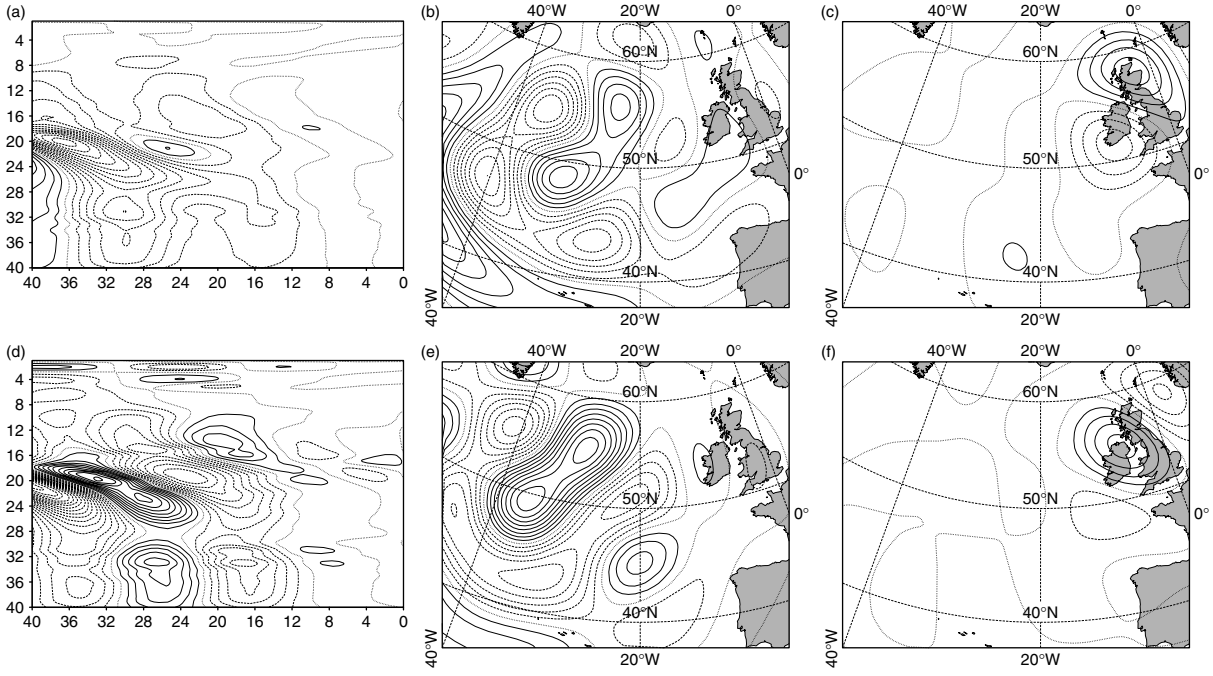

Figure 13. Singular vectors for the ECMWF forecast in terms of relative vorticity. For singular vector 1, (a) shows a vertical cross-section along latitude 45 °N, from 40 °W to 0 °W, and (b) is the initial and (c) the evolved singular vector at model level 13 (around 300 hPa). (d–f) are as (a–c), but for singular vector 2. Solid lines denote positive values and dashed lines negative values. The order of magnitude is 10^{-7} with contour interval 2×10^{-8} for the initial perturbations, and 10^{-5} with contour interval 2×10^{-6} for the evolved perturbations.

DOI: 10.1002/qj

29 and 30. These members form a pair that result from perturbations of opposite sign. The corresponding difference is located in the jet stream region, both in the mismatch area and in the trough at 10 °W. For this particular pair, the member with the strongest development (member 30) has lower values of the potential vorticity at upper levels and larger values of potential vorticity at lower levels, when compared with the control forecast. In Figure 14(a–c) difference fields are shown relating ensemble member 30 to the control forecast. (The fields for ensemble member 29 have opposite sign.) The maximum difference with the control run is 1.25 PVU. Next in terms of extreme behaviour is ensemble pair 43 and 44, which have the same overall properties as the previous pair. The following pair is 41 and 42. For the member with the strongest development (member 42), the situation is now quite different as the potential vorticity at upper levels is higher and the potential vorticity at lower levels is lower than the control forecast. Difference fields for member 42 are shown in Figure 14(d–f). (The difference fields for member 41 have opposite sign.) Figure 14 indicates, and study of the other pairs of ensemble members confirms, that the member which displays a stronger development of the cyclone is usually characterized by a somewhat lower msl pressure at the centre of the incipient cyclone.

The pair of ensemble members 41 and 42 is of most interest to our case. The corresponding msl pressures at the cyclone's centre are displayed in Figure 4(b). Ensemble member 42, if compared with the control forecast, constitutes a modest improvement of the match between potential vorticity field and water vapour image, as can be seen by comparing the two panels of Figure 12. It also has a somewhat lower msl pressure at the centre of the incipient cyclone which, as we shall see in the next section, is supported by some observational evidence. It finally leads to a deeper cyclone at +18 h. It is therefore of some interest to compare the development of these two members which, at +18 h, give either a surface low that is shallower (member 41) or one that is deeper (member 42) than the control forecast. These differences are illustrated by Figure 4 and by Figure 11(d–i). The time evolution in terms of the potential vorticity at upper and lower levels for this pair of members is shown in Figures 15 and 16, respectively.

Note that the difference in development between these two members is mostly associated with the flow at upper levels. In ensemble member 42, the potential vorticity at 315 K forms a rather strong anomaly to the south-west of Ireland at +18 h, an anomaly that is absent in ensemble member 41. The development of the potential vorticity at lower levels is almost identical in these two members. The deeper surface low that emerges in ensemble member 42 can thus be ascribed to the development of an anomaly in potential vorticity at upper levels. (The somewhat larger scale of the potential vorticity at lower levels, as compared with Figure 7, is caused by the coarser spatial resolution of the ECMWF model used in the ensemble calculations.)

5. Discussion

The deepening of the cyclone in the original HIRLAM run clearly touches the outer edge of the ECMWF ensemble. On the other hand, the cyclone's centre follows a path

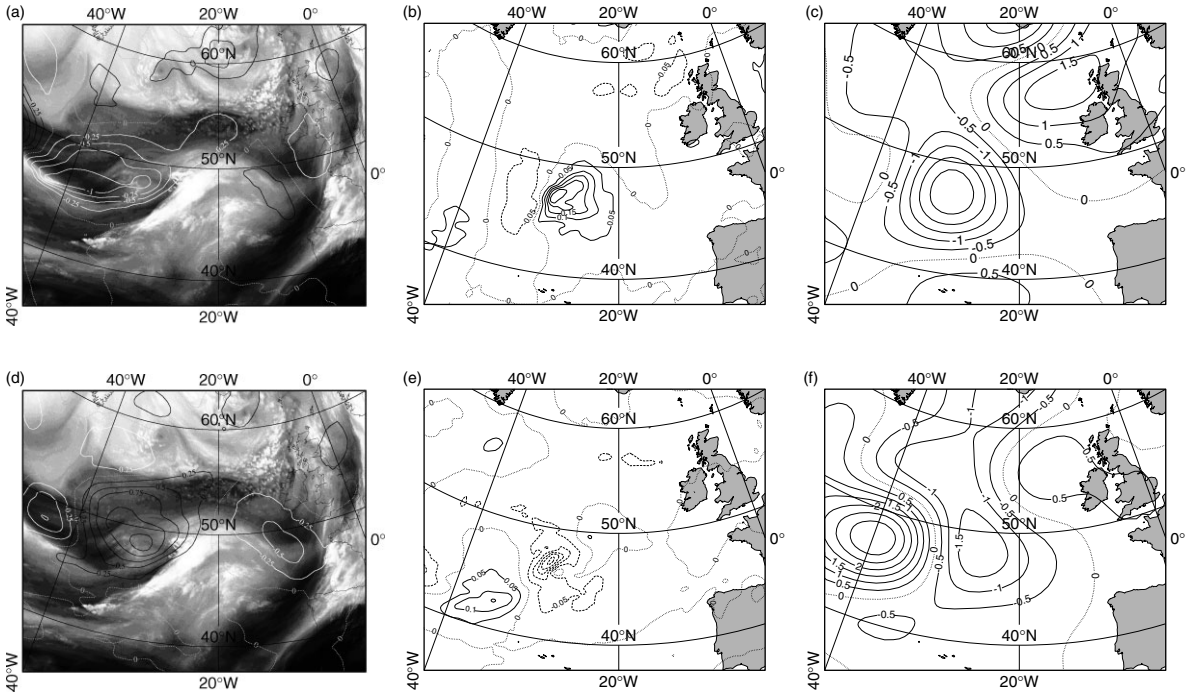

Figure 14. Difference fields with respect to the control forecast for ensemble member 30: (a) potential vorticity on the 315 K surface, (b) potential vorticity on model level 34 (around 925 hPa) and (c) msl pressure. (d–f) are as (a–c), but for ensemble member 42. The fields of ensemble members 29 and 41 have signs opposite to those of members 30 and 42, respectively. The units are as before.

DOI: 10.1002/qj

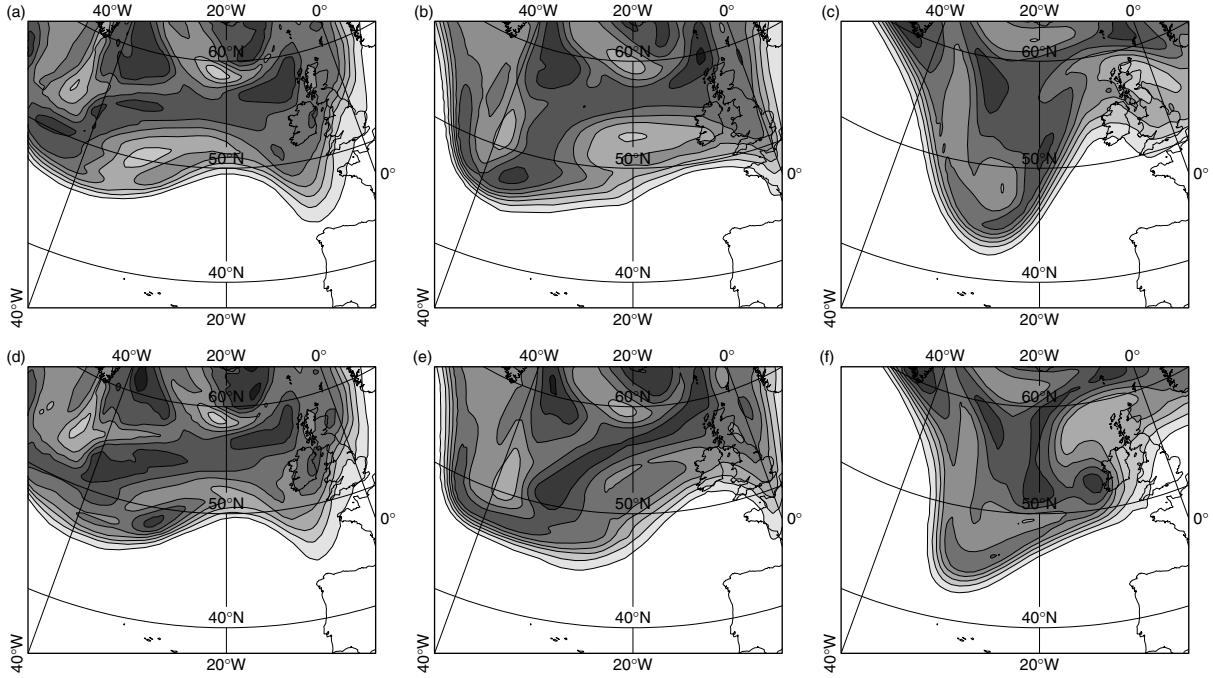

Figure 15. As Figure 6, but for (a–c) ECMWF ensemble member 41 and for (d–f) ensemble member 42.

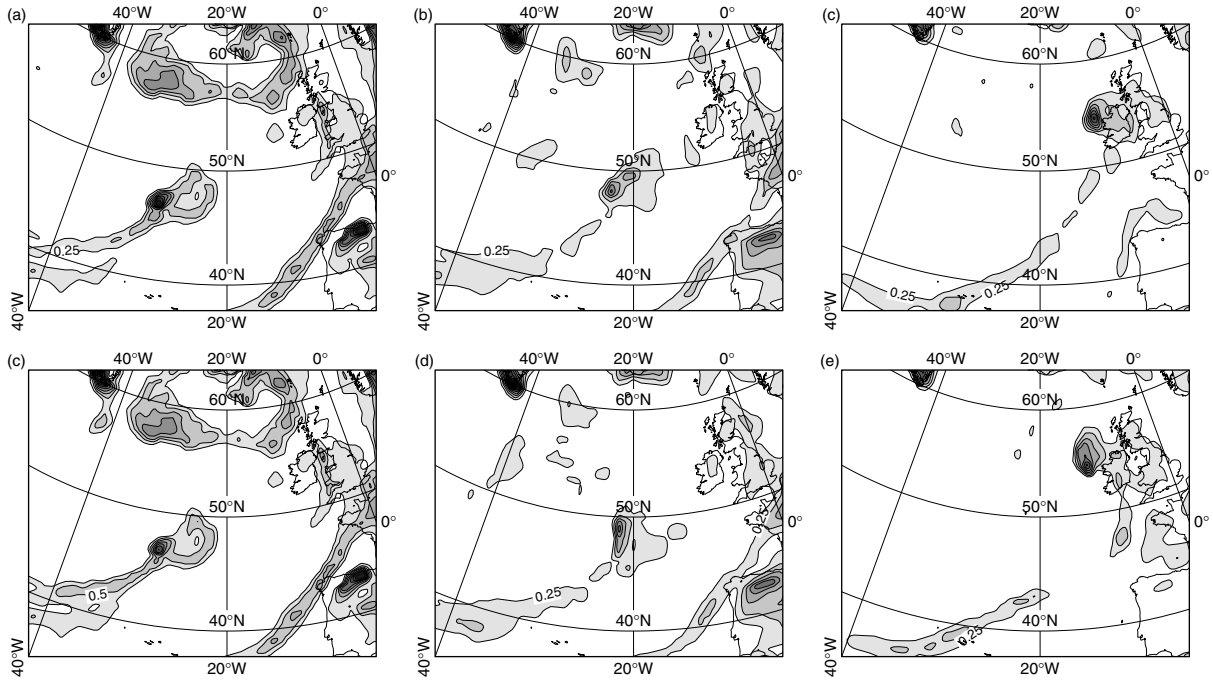

Figure 16. As Figure 7, but with contour interval 0.25 PVU, and shading from 0.25 PVU; (a–c) for ECMWF ensemble member 41, and (d–f) for ensemble member 42.

close to the ensemble mean. The runs that result from modifications exp1 and exp3 are close to the ensemble mean, both in terms of the strength and the position of the cyclone. In modification exp2, the deepening of the cyclone resembles the ensemble mean, but the position lies at the outer edge of the ensemble. All modifications that are discussed, including exp1a to exp1d, trop1 and trop2, are within the limits that the ECMWF ensemble has indicated, which means that they are inside the range of acceptable possibilities.

We have noticed that the most successful HIRLAM modification, like ECMWF ensemble member 42 leading to a deeper depression at +18 h, is characterized by a reduced msl pressure at the centre of the initial cyclone. To investigate whether there is observational evidence for a reduced msl pressure at the centre of the cyclone we consider ship observations at 00 UTC. In Figure 17, the original ECMWF analysis, the original HIRLAM analysis and the ship observations are plotted on the background of the (infrared) satellite picture.

DOI: 10.1002/qj

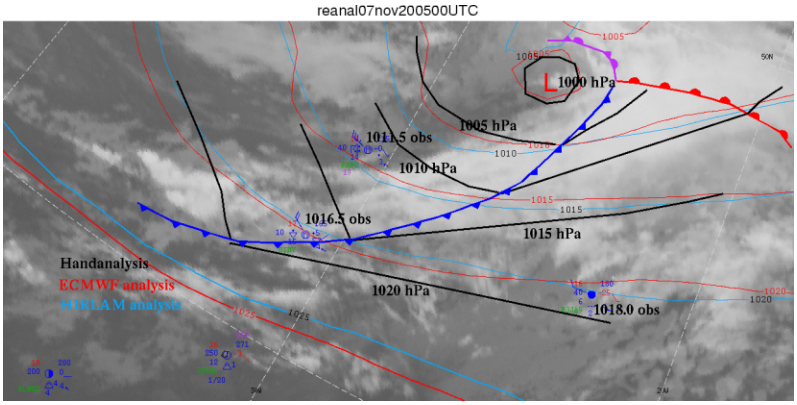

Figure 17. Hand analysis of the pressure field at 7 November 2005, 00 UTC, showing cold front (blue), warm front (red) and occlusion (purple) and isobars (black). The isobars were moved somewhat to the south compared with the HIRLAM and ECMWF analyses (blue and red isobars, respectively). They were also made to change direction at the assumed cold front. The overall result is a reduced pressure of about 5 hPa in the core of the incipient cyclone. The changes are based on three ship observations, marked by 'obs'. This figure is available in colour online at www.interscience.wiley.com/qj

It is clearly seen that, compared to the ships DIDY (position 42.24 °N, 31.00 °W; observed pressure 1016.5 hPa), P3JAG (position 44.00 °N, 22.54 °W; observed pressure 1018.0 hPa) and KRPD (position 44.36 °N, 30.40 °W; observed pressure 1011.5 hPa), both models have msl pressure which is too high. The overlaid hand analysis tries to capture the position and orientation of the cold front and isobars consistent with those three ship observations. This supports the view that, in this case, modifications of the analysis that reduce the msl pressure bring the analysis closer to the observations.

The barotropic shift that characterizes exp1, in which the flow at both upper and lower levels is modified, not only improves the analysis at upper levels but also produces the right changes at lower levels to generate a forecast that is essentially correct in terms of msl pressure. To the question why this is so, our answer is non-committal: expressed in terms of potential vorticity, the modification has, apparently, brought the different structural elements in a configuration better equipped for rapid deepening of the cyclone. This is confirmed by the fact that the modification resembles the strongly developing ensemble member 42 with which it shares the higher values of the potential vorticity at upper levels and the lower values of the potential vorticity at lower levels and, in addition, the lower values of the msl pressure in the centre of the incipient cyclone. It is important to note that there are ensemble members (such as member 29, of which the difference with the control forecast can be seen in Figure 14(a–c), signs reversed) that have larger values of the potential vorticity at upper levels – and would thus improve the fit with the water vapour image – but produce a forecast that is worse. But member 29 (see again Figure 14(a–c), signs reversed) has higher values of the msl pressure at the centre of the cyclone at analysis time, in contradiction to the ship observations discussed above, and therefore does not improve the analysis at mean sea level.

Of course, in a study like this, we have the benefit of hindsight; we know how the flow has evolved in reality and we are in a position to check whether modifications of the initial state improve the development. Singular vectors and ensembles are useful as they bring to light the different alternatives that are allowed by the uncertainty of the analysis. On the other hand, the type of perturbations our method generates have the advantage that they are of a relatively simple nature and inspired by water vapour satellite images with their high spatial and temporal resolution. It remains to be seen, though, how in an operational environment – in which there is no benefit of hindsight – the modifications can be used effectively. We conjecture that the method might be most useful if singular vectors are available at analysis time. Before applying a modification to the full nonlinear model, we might then first project it onto the singular vectors to investigate, in a linearized approximation, what the effect of the modification will be. It is then probably easier to guess in advance whether a modification is likely to lead to a better forecast. A somewhat different line of approach is discussed by Homar *et al.* (2006). These authors have shown that human intervention could contribute positively to the generation of a short-range ensemble. There, sensitive areas for the development of severe weather were identified and an ensemble was created that has better statistics. Therefore, it is worthwhile to investigate our method further in the light of short-term ensemble generation.

6. Conclusions

Application to a case of rapid cyclogenesis over the Atlantic Ocean has shown that the potential vorticity modification method developed by Verkley *et al.* (2005) makes it possible to improve the analysis and corresponding forecast by a limited-area model such as HIRLAM. The model predicted a deepening depression at the right location but the amount of deepening was too small compared with the verifying analyses. However, quite a few trials were needed to find a modification that put the HIRLAM forecast on the right track. The

DOI: 10.1002/qj

most successful modification consisted of a barotropic, column-wise, shift of the jet stream to lower latitudes that brings the potential vorticity field at 315 K closer to the water vapour satellite image and reduces the msl pressure beneath. Observational evidence at analysis time in the form of pressure measurements by ships corroborated these lower msl pressures. The modification, called exp1, was analysed in terms of the difference fields at analysis time and in terms of differences in subsequent development. The deeper cyclone at +18 h that characterizes the modified run is mainly the result of a more strongly growing potential vorticity structure at lower levels. It was noticed that the stronger growth at lower levels is accompanied by larger amounts of precipitation, but how exactly the modification has accomplished this stronger growth has not become clear. Several alternative modifications were discussed to study the sensitivity of the forecast to the modification applied.

We also studied the problem from the perspective of the ECMWF global forecast model. Although the mismatch between potential vorticity field and water vapour image is only slightly less in the ECMWF analysis than in the HIRLAM analysis, the ECMWF model predicted the development of the cyclone's position and msl pressure very well. Calculation of ECMWF singular vectors, with an optimization time of 24 h and targeted at the region where the cyclone ends up after 24 h, has shown that the flow is quite sensitive to perturbations in the initial condition, in particular in the region of the mismatch. The singular vectors furthermore showed that this sensitivity is not limited to upper levels alone, in accordance with the study by Røsting *et al*. (2003). We also considered the operational ECMWF ensemble. It has become clear that the HIRLAM forecast is at the edge of the ECMWF ensemble and that our most successful modification, exp1, has brought the forecast closer to the ensemble mean. All modifications studied were within the limits that the ECMWF ensemble has indicated.

When ordered in terms of decreasing extremity in msl pressure development, pair 41 and 42 of the ECMWF ensemble is the first pair in which the member with the strongest development (42) had properties in accordance with observational evidence: higher values of the potential vorticity at upper levels and lower values of the msl pressure at the centre of the incipient cyclone. With its somewhat lower values of the potential vorticity at lower levels, it quite closely resembles the most successful modification exp1. The difference in development between the members 41 and 42 was studied in terms of potential vorticity at upper and lower levels.

Concerning future development of the method, we conjecture that further progress might be possible if singular vectors are available at analysis time. The method might then possibly lead, not unlike the approach of Homar *et al*. (2006), to the generation of a small ensemble of alternative forecasts, based on modifications that are synoptically realistic as well as dynamically effective.

Acknowledgements

The research was funded by the Netherlands Agency of Aerospace Programmes (NIVR). The authors would like to thank Dr J. Barkmeijer for fruitful discussions, singular vector computations and the generation of ensembles. Dr A.B.C. Tijm is thanked for his interest in our work. We are grateful to Mrs X. Wang for her contribution to the graphical interface and to Dr A.H. Verhoef for his help in processing the satellite images. Mr G. Groen is thanked for helping us in interpreting the ship observations and producing the hand analysis in Figure 17. The constructive comments of Dr P. Clark and two anonymous reviewers have helped us in giving the manuscript its present form.

Appendix

Overview of experiments

In this appendix we give two tables with additional information on the different modifications and runs that were performed in the course of this study. Table A.I summarizes the different parameters of the modifications, and Table A.II gives information on the positions and central pressures of the developing cyclone.

References

Buizza R, Palmer TN. 1995. The singular vector structure of the atmospheric global circulation. *J. Atmos. Sci.* **52**: 1434–1456.

Davis CA, Emanuel KA. 1991. Potential vorticity diagnostics of cyclogenesis. *Mon. Weather Rev.* **119**: 1929–1953.

Table A.I. Overview of modification parameters. The most successful modification is exp1.

Experiment	From	To	Radius (°)	α	Vertical structure
exp1	48.8N 32.0W	46.0N 30.3W	8	2	uniform
exp2	50.0N 34.0W	46.0N 32.0W	10	2	uniform
exp3	49.5N 32.0W	46.5N 31.0W	10	2	uniform
exp1a	49.0N 33.0W	46.0N 31.0W	8	2	uniform
exp1b	50.0N 32.0W	47.0N 30.0W	8	2	uniform
exp1c	49.0N 31.0W	46.0N 29.0W	8	2	uniform
exp1d	51.0N 32.0W	48.0N 30.0W	8	2	uniform
trop1	48.8N 32.0W	46.0N 30.3W	8	2	135 to 465 hPa, max at 240 hPa
trop2	48.8N 32.0W	46.0N 30.3W	8	2	135 to 645 hPa, max at 300 hPa

DOI: 10.1002/qj

Table A.II. Position and central msl pressure of the depression. The accuracy of the positions is estimated to be 0.1°, and the accuracy of the pressure values to be 0.2 hPa. The last three rows concern the control forecast and members 41 and 42 of the ECMWF ensemble.

Experiment	00	+6	+12	+18	+24
HIRLAM an	47.7N, 27.0W 1003.8	49.7N, 20.1W 997.2	52.9N, 14.6W 987.7	56.1N, 11.7W 974.9	58.2N, 9.5W 969.7
ECMWF an	47.1N, 28.7W 1003.3	49.5N, 20.8W 995.5	52.3N, 14.9W 985.0	55.4N, 10.8W 974.5	57.9N, 7.7W 974.0
HIRLAM fc	47.7N, 27.0W 1003.8	49.6N, 20.3W 997.7	52.0N, 14.6W 991.7	55.2N, 10.8W 984.3	58.3N, 7.3W 981.3
ECMWF fc	47.1N, 28.6W 1003.3	49.1N, 21.6W 993.8	52.1N, 15.5W 983.0	55.3N, 11.5W 972.6	58.2N, 7.7W 970.3
exp1	47.6N, 26.7W 1001.4	49.3N, 20.6W 991.6	52.4N, 15.8W 984.8	55.2N, 12.8W 976.0	58.1N, 10.8W 968.9
exp2	47.8N, 26.7W 1002.1	49.6N, 20.7W 992.0	52.4N, 16.7W 987.0	55.8N, 13.5W 981.9	58.9N, 12.7W 975.5
exp3	47.6N, 26.9W 1001.4	49.6N, 20.8W 990.0	52.3N, 16.3W 984.1	55.3N, 13.4W 976.2	57.9N, 11.7W 966.2
exp1a	47.6N, 26.8W 1001.4	49.7N, 20.6W 990.9	52.7N, 16.1W 983.7	55.8N, 13.5W 976.2	58.3N, 11.9W 966.2
exp1b	47.6N, 26.8W 1001.0	49.3N, 20.9W 990.4	52.4N, 15.8W 983.4	55.2N, 13.1W 974.6	57.5N, 11.0W 965.6
exp1c	47.6N, 26.9W 1003.6	49.2N, 20.9W 994.5	51.9N, 15.6W 989.1	55.1N, 12.1W 980.3	58.2N, 10.1W 970.1
exp1d	47.6N, 26.9W 999.7	49.6N, 20.8W 989.0	52.5N, 16.2W 981.6	55.2N, 13.6W 973.8	57.5N, 11.2W 966.6
trop1	47.7N, 27.2W 1001.7	49.8N, 20.5W 994.2	52.3N, 15.6W 989.2	55.4N, 12.3W 982.3	58.3N, 10.2W 974.7
trop2	47.7N, 27.2W 1001.7	49.9N, 20.3W 993.0	52.7N, 15.4W 987.8	55.9N, 12.0W 981.6	58.8N, 9.7W 976.2
control	47.1N, 28.6W 1004.1	49.0N, 21.9W 995.1	51.8N, 16.0W 984.7	54.9N, 11.5W 975.0	57.9N, 8.7W 969.3
member 41	47.1N, 28.8W 1005.7	49.0N, 22.6W 998.3	51.4N, 16.0W 990.4	54.5N, 11.2W 985.2	58.1N, 7.6W 979.7
member 42	47.4N, 28.2W 1002.8	49.3N, 21.7W 991.6	51.8N, 16.7W 979.7	54.5N, 12.7W 969.9	56.7N, 9.8W 967.0

Demirtas M, Thorpe AJ. 1999. Sensitivity of short-range weather forecasts to local potential vorticity modifications. *Mon. Weather Rev.* **127**: 922–939.

Gustafsson N, Berre L, Hörnquist S, Huang XY, Lindskog M, Navascués S, Mogensen KS, Thornsteinsson S. 2001. Three-dimensional variational data assimilation for a high-resolution limited-area model. Part I: General formulation and the background-error constraint. *Tellus* **53A**: 425–446.

Haltiner GJ, Williams RT. 1980. *Numerical prediction and dynamic meteorology*. J. Wiley and Sons: New York.

Homar V, Stensrud DJ, Levit JJ, Bright DJ. 2006. Value of human-generated perturbations in short-range ensemble forecasts of severe weather. *Weather Forecasting* **21**: 347–363.

Hoskins BJ, McIntyre ME, Robertson AW. 1985. On the use and significance of isentropic potential vorticity maps. *Q. J. R. Meteorol. Soc.* **111**: 877–947.

Hoskins BJ, Buizza R, Badger J. 2000. The nature of singular vector growth and structure. *Q. J. R. Meteorol. Soc.* **125**: 1565–1580.

Leutbecher M, Palmer TN. 2007. *'Ensemble forecasting'. Technical Memorandum* 514. ECMWF Reading, UK.

Lindskog M, Gustafsson N, Navascués S, Mogensen KS, Huang XY, Yang X, Andræ U, Berre L, Thornsteinsson S, Rantakokko J. 2001. Three-dimensional variational data assimilation for a high-resolution limited-area model. Part II: Observation handling and assimilation experiments. *Tellus* **53A**: 447–468.

Molteni F, Buizza R, Palmer TN, Petroliagis T. 1996. The ECMWF ensemble prediction system: methodology and validations. *Q. J. R. Meteorol. Soc.* **122**: 73–119.

Røsting B, Kristjánsson JE, Sunde J. 2003. The sensitivity of numerical simulations to initial modifications of potential vorticity – a case-study. *Q. J. R. Meteorol. Soc.* **129**: 2697–2718.

Røsting B, Kristjánsson JE. 2006. Improving simulations of severe winter storms by initial modification of potential vorticity in sensitive regions. *Q. J. R. Meteorol. Soc.* **132**: 2625–2652.

Santurette P, Georgiev C. 2005. *Weather analysis and forecasting*. Elsevier Academic Press.

Swarbrick SJ. 2001. Applying the relationship between potential vorticity fields and water vapour imagery to adjust initial conditions in NWP. *Meteorol. Appl.* **8**: 221–228.

Undén P, Rontu L, Järvinen H, Lynch P, Calvo J, Cats G, Cuxart J, Eerola K, Fortelius C, Garcia-Moya JA, Jones C, Lenderink G, McDonald A, McGrath R, Navascués B, Nielsen NW, Ødegaard V, Rodriguez E, Rummukainen M, Rööm R, Sattler K, Sass BH, Savijärvi H, Wichers Schreur B, Sigg R, The H, Tijm A. 2002. 'HIRLAM-5 Scientifc Documentation'. Available from the HIRLAM-5 project, c/o Per Undén, SMHI, S-601, 76 Norrköping, Sweden.

Verkley WTM, Vosbeek PWC, Moene AR. 2005. Manually adjusting a numerical weather analysis in terms of potential vorticity using three-dimensional variational data assimilation. *Q. J. R. Meteorol. Soc.* **131**: 1713–1736.

Wernli H, Dirren S, Liniger MA, Zillig M. 2002. Dynamical aspects of the life cycle of the winter storm 'Lothar' (24–26 December 1999). *Q. J. R. Meteorol. Soc.* **128**: 405–429.

DOI: 10.1002/qj